Materials Today Communications 26 (2021) 101694

Contents lists available at ScienceDirect

Materials Today Communications

journal homepage: www.elsevier.com/locate/mtcomm

On the molecular properties of graphene-pyrazines conjugated Ru and Fe complexes: Computational insights

Abdulilah Dawoud Bani-Yaseen

Department of Chemistry & Earth Sciences, College of Arts &Science, Qatar University, Doha, P.O. Box 2713, Qatar

ARTICLE INFO

Keywords:
Graphene
Metal complexes
Electrocatalysts
Heterogenization
Density functional calculations

ABSTRACT

Graphene and related materials can exhibit substantial molecular properties of significant importance in various landscapes of interests including catalysis. On the other hand, transition-metal-based molecular heterogeneous electrocatalysts can demonstrate enhanced catalytic usability compared to homogeneous analogues concerning recoverability and durability. We present in this study computational investigations on selected molecular properties graphene-based heterogenized molecular complexes of the (2,2′-bipyridyl)-metal complexes, $[M(bpy)_3]^{2+}$ (M = Fe, Ru). The computational study was conducted using the density functional theory (DFT) approach with an implicit solvation model (IEFPCM). Interestingly, the DFT results revealed that the key structural properties of the complexes are not disrupted by heterogenization. Also, the DFT-based calculated reduction potential of all examined species revealed a good agreement between the graphene-based heterogeneous electrocatalysts and their corresponding homogeneous analogues in terms of the redox potentials and the corresponding molecular properties in implicit acetonitrile. The finding reported herein demonstrates the applicability of graphene in covalent heterogenization of a molecular catalyst. As such, these computational insights can be useful in future efforts toward developing efficient heterogeneous molecular catalysts for a wide range of important chemical transformations.

1. Introduction

Electrocatalysis is considered as the favored catalytic method for the chemical transformation of various substances of environmental and energy importance [1–7], such as the electrocatalytic reduction of CO_2 [2,5]. Conventionally, electrocatalytic reduction of such substances is a feasible path that could be accomplished via applying transition-metal-based catalysts under particular electrical biases. Consequently, such electrocatalysts require relatively large electrical overpotential to undertake the chemical reactions of interest. As such, several types of electrocatalysts have been recently developed toward affording a wide spectrum of catalytic chemical transformations within the landscapes of homogeneous and heterogeneous catalysis [8–20].

Utilization of heterogeneous catalysis can offer several operational advantages compared to homogeneous analogues; this includes that the catalyst can be separated easily from the products regardless of the phase of the system. Furthermore, it exhibits a higher selectivity to the desired product at a realistic conversion level. However, the heterogeneous catalyst has some drawbacks; for example, it suffers from relatively low activity due to the limitation of exposed active sites. The catalytic performance tunability is low and multiple active sites are other drawbacks in such heterogeneous catalysis. On the other hand, molecular homogeneous catalysis can offer superior advantages concerning selectivity toward specific types of chemical reactions. For this reason, there is a growing interest toward building up a catalytic system that comprises the two phase-based catalysis toward reducing the drawbacks of each type. Interestingly, molecular heterogeneous catalysis can provide interesting operational conditions that can combine the features of both heterogeneous and homogeneous catalysis [1–9].

The applicability of graphene in a wide spectrum of applications has been broadly demonstrated including catalysis [21–28]. Commonly, in catalysis, graphene and related materials have been generally utilized as stand-alone catalysts or within a matrix of a heterogeneous catalytic process in which graphene moiety acts as a support for other catalysts [29–38]. In heterogeneous catalysis, the substantial performance of graphene-based materials has been demonstrated in catalyzing a wide spectrum of chemical transformations for various applications, such as cross-coupling reactions [33,39,40], oxygen reduction in fuel cell [41–43], hydrogen evolution reaction [44–46], and reduction of carbon dioxide (CO_2) into various products [38,47,48]. It is noteworthy

E-mail address: abdulilah.baniyaseen@qu.edu.qa.

https://doi.org/10.1016/j.mtcomm.2020.101694
Received 30 July 2020; Received in revised form 10 September 2020; Accepted 18 September 2020
Available online 28 September 2020

mentioning that graphene-based materials can exhibit characteristic features that can enhance the feasibility of such catalyzed chemical reactions; these features include a substantial electronic structure with zero bandgap and high electrical conductivity.

However, it is noteworthy to mention that homogeneous catalysis can still offer more superior catalytic efficiency compared to the heterogeneous counterparts, which is attributed to the availability of active sites. In principle, for homogeneous catalysis, a molecular catalyst of transition metal is used where the high availability of active sites is encountered. On the other hand, heterogenization of molecular catalysts can be generally accomplished via the immobilization of a homogeneous catalyst through mainly two approaches depending on the type of interaction used to bind the active site to the surface, namely covalent and noncovalent bondings [49–55]. In the noncovalent method, the inorganic or organometallic complexes could be physisorbed into various types of a carbon-based electrode; such as graphene and graphite. Consequently, noncovalent immobilization uses complexes having an aromatic substituent and they might interact with carbon electrode through π-π stacking interactions. In covalent immobilization, it possesses a covalent bond between the metal-based complex and the solid surface with a stable linkage. To this end, a growing interest has recently grown in merging molecular catalysts with graphene-based materials through a heterogenization process. These interests are mainly focused on experimental research focusing on the immobilization of molecular catalysts on the surface of a solid substrate [49,56–60]. For example, Blackmore et al. reported on the noncovalent immobilization of rhodium proton-reduction catalyst [Cp*Rh(P)Cl]Cl on a graphitic electrode utilizing pyrene-appended bipyridine ligand (P) as a linker between the surface of the electrode and the molecular catalyst [49]. Recently, Surendranath et al. communicated on the production of a molecular heterogeneous catalyst of metals-centered (M = Ru,Rh) catalysts immobilized covalently on a graphite-conjugated catalyst both connected via a pyrazine linkage [55]. Nevertheless, it can be noted several reported studies lack some important information concerning the molecular properties of the catalysts of interest. As such, it is noteworthy to emphasize on the significance of providing insights at the molecular level concerning the behavior of such electrocatalysts toward enhancing their catalytic performance.

We provide in this study molecular insights concerning the redox and molecular properties of metal-based graphene-modified electrocatalysts. We particularly investigated computationally the effect of immobilization of molecular catalysts $[M(bpy)_3]^{2+}$, M = Ru, Fe; bpy = bipyridine, on graphene concerning their molecular properties. We performed density functional theory (DFT) calculations concerning the catalytic reduction potentials for both the graphene-based heterogenized molecular catalysts and their corresponding homogeneous analogues. The effect of heterogenization is interpreted and discussed in terms of selected molecular properties of the corresponding electrocatalysts.

2. Computational methods

All calculations were conducted using Gaussian09 software package, Revision E.01 [61].

Geometry optimization was performed using the DFT-B3LYP method employing the 6−31+G(d) and lanl2dz basis set for the non-metal and metal atoms, respectively. The solvent effect was examined implicitly using the integral-equation formalism polarizable continuum model (IEFPCM) [62]. The calculations of geometry optimization were followed accompanied by frequency calculations to assure that the optimized geometry is at a local minimum. All geometries were optimized in the gas phase followed by optimization in acetonitrile employing the IEFPCM approach at the same level of theory. Acetonitrile was selected as proof of principle concerning the effect of solvent on the examined molecular properties of the substances considered in this work. Also, acetonitrile is a key organic solvent with medium polarity and is widely used in catalyzed organic reactions due to its exceptional solvation ability of a wide spectrum of materials compared to other polar and nonpolar solvents. The heterogenized molecular catalyst is modelled as illustrated in Fig. 1. This model comprises graphene sheet, pyrazine as a linker, and the homogeneous molecular complex of transition elements.

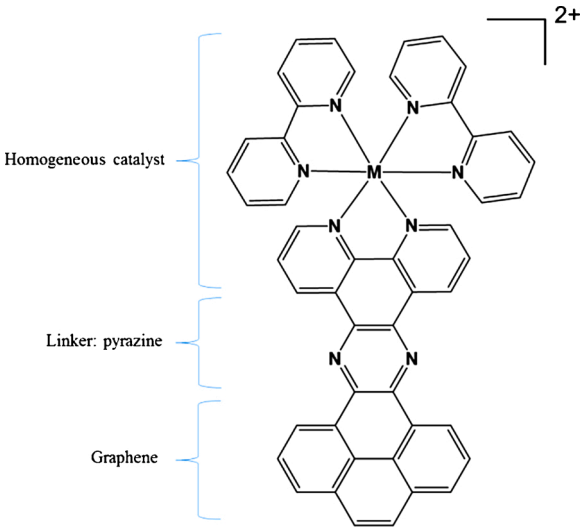

Fig. 1. Structure of the immobilized catalyst $[M(bpy)_3]^{2+}$-G_r; M = Ru, Fe; bpy = bipyridine.

$$[ML]_g^{2+} + e^- \xrightarrow{\Delta G^\circ_{Red,g}} [ML]_g^{1+}$$

$$\Delta G^\circ_{sol}(ox) \qquad\qquad \Delta G^\circ_{sol}(red)$$

$$[ML]_{sol}^{2+} + e^- \xrightarrow{\Delta G^\circ_{Red,sol}} [ML]_{sol}^{1+}$$

Scheme 1. Born−Haber thermodynamic cycle for computing the 1-e reduction potential of $[ML]^{n+}$ in solution.

It is noteworthy mentioning that the pyrazine moiety can offer a robust aromatic linkage with strong electronic coupling between the graphene sheet and the molecular complex [55,63]. Hence, such strong electronic coupling is crucial toward enhancing the catalytic performance of heterogenized molecular catalysts of interest [57,64]. Importantly, it has been previously demonstrated experimentally and computationally that the reactivity of edges of graphene is much higher than the bulk counterpart [65,66]. As such, we excluded the graphene-bulk from our study, and we considered only the edge-covalent modification of graphene. On the other hand, it is worth noting that modelling the graphitic moiety with four fused-rings of benzene offers reasonable representation for the covalently-modified surface of graphene and importantly less expensive computational experiments. Such an approach is well in line with previously reported results concerning molecular aspects of graphitic-based materials, where the addition of more fused rings does not affect the quality of the results [64].

Redox potential calculations. The Born-Haber thermodynamic cycle was employed to calculate the redox potential of the optimized geometries of the compounds of interest in the corresponding medium [67–69]; see Scheme 1.

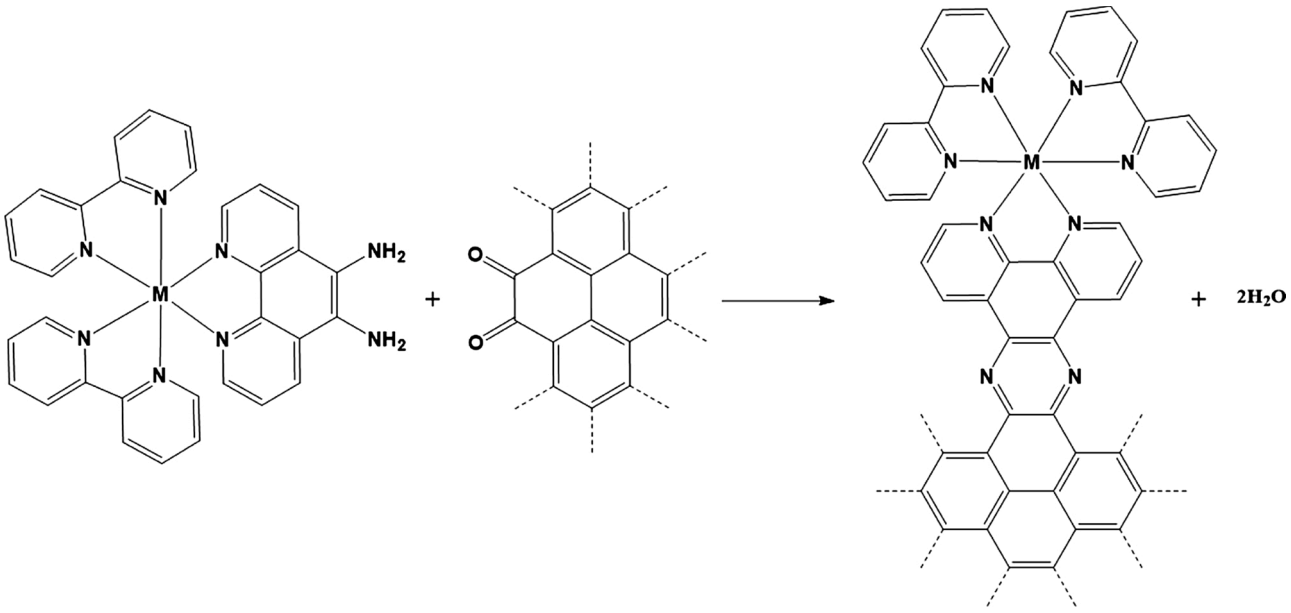

Scheme 2. Key synthetic step of $[M(bpy)_3]^{2+}$-G_r (M = Ru, Fe).

The standard Gibbs free energy (G°) of all examined species was obtained from the frequency calculations as implemented Gaussian09 software package. According to the cycle shown in Scheme 1, the change in the standard Gibbs free energy associated with the reduction step in solution ($\Delta G^\circ_{Red.sol}$) can be calculated via employing eq.1, and consequently $\Delta G^\circ_{Red.sol}$ can be used to calculate the reduction potential in volt unit ((E°(V)) versus a saturated calomel electrode (SCE) via employing eq.2.

$$\Delta G^\circ_{Red,sol} = \Delta G^\circ_{Red,g} + \Delta G^\circ_{sol.}\,(red) - \Delta G^\circ_{sol.}(ox) \quad (1)$$

$$\Delta E^\circ(V) = \Delta G^\circ_{(red,sol)}/\,(nF) - SCE \quad (2)$$

where, $\Delta G^\circ_{Red,sol}$ and $\Delta G^\circ_{Red,g}$ are the changes in Gibbs free energy associated with the reduction process of the molecules in a solvent of interest and the gas phase, respectively; ΔG°_{sol} (red.) and ΔG°_{solv} (ox) are the changes in Gibbs free energy of solvation for the reduced and oxidized forms of the molecule; respectively; n is the number of electrons involved in the redox process; F is the Faraday constant.

3. Results and discussion

It is noteworthy mentioning that covalent functionalization offers a great opportunity toward enhancing the molecular properties of graphene. In such an approach the molecular catalyst is covalently attached to the graphene sheet. Indeed, this approach is tremendously challenging due to the high stability of graphene. However, with the aid of synthetic chemistry methods such as condensation reactions, covalent functionalization of graphene has become more feasible. Recently, the condensation reaction of 1,2-phenylenediamines with ortho-quinone edge sites of graphite has been reported by Surendranath and coworkers [70]. It can be suggested that such a reaction may mechanistically proceed via a typical condemnation reaction. Thus, it is prospectively anticipated that a molecular catalyst such as $[M(bpy)_3]^{2+}$ (M = Ru, Fe; bpy = bipyridine) can be chemically modified to be covalently linked to the graphene sheet as illustrated in scheme 2 .

To this end, the focus of this work is to provide insights into the molecular and electrochemical properties of the graphene-based heterogenized molecular catalyst of selected transition elements and compare it with the features of their homogenous analogues in terms of

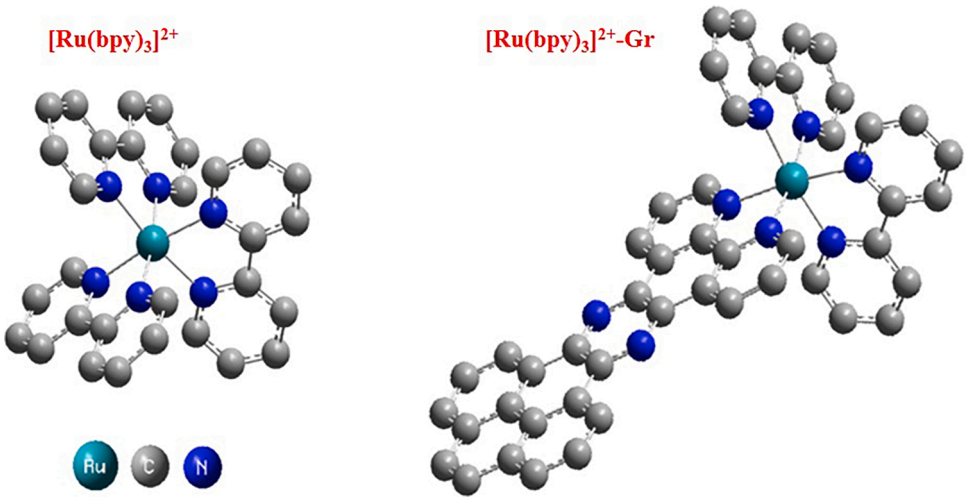

Fig. 2. Optimized geometry of $[Ru(bpy)_3]^{2+}$ and $[Ru(bpy)_3]^{2+}$–G_r in acetonitrile; hydrogen atoms are omitted for clarity.

Table 1
Geometrical parameters of the optimized geometries of $[M(bpy)_3]^{2+}$ complexes and their corresponding graphene-based heterogenized analogues.

Ru								
	$[Ru(bpy)_3]^{2+}$		$[Ru(bpy)_3]^{2+}$-G_r		$[Ru(bpy)_3]^{1+}$		$[Ru(bpy)_3]^{1+}$-G_r	
	Vac.	AcNt	Vac.	AcNt	Vac.	AcNt	Vac.	AcNt
Bond Length (Å)								
Avg. Ru-N	2.118	2.112	2.119	2.114	2.106	2.107	2.108	2.113
Bond Angle (°)								
N1-Ru-N2	78	78	78	78	78	78	78	79
N3-Ru-N4	78	78	78	78	78	78	78	78
N5-Ru-N6	78	78	78	78	78	78	78	78
N2-Ru-N3	88	89	88	88	90	89	89	88
Fe								
	$[Fe(bpy)_3]^{2+}$		$[Fe(bpy)_3]^{2+}$-G_r		$[Fe(bpy)_3]^{1+}$		$[Fe(bpy)_3]^{1+}$-G_r	
	Vac.	AcNt	Vac.	AcNt	Vac.	AcNt	Vac.	AcNt
Bond Length (Å)								
Avg. Fe-N	2.024	2.017	2.025	2.020	2.012	2.014	2.015	2.018
Bond Angle (°)								
N1-Fe-N2	81	81	82	81	81	81	82	82
N3-Fe-N4	81	81	81	81	81	82	82	81
N5-Fe-N6	81	81	81	81	81	81	82	81
N2-Fe-N3	89	89	89	89	90	89	89	89

the structural properties, atomic charges, and molecular orbitals. Importantly, this work does not include the examination of changing the computational method used; like studying the effect of changing the DFT functional, basis set, or the solvation method used. On the other hand, the theory and models used in this work is consistent with the theories used in previously published work in the area focused on studying the molecular and electrochemical features of metal-based complexes.

Geometry optimization. It is noteworthy to mention that the geometry optimization is a key step toward investigating selected molecular properties of the materials of interest. Importantly, it is essential to optimize the geometry of the $[M(bpy)_3]^{2+}$ complexes before and after heterogenization in order to assess the retainability of the molecular structure of the complex. Starting with geometry optimization, we optimized the geometry of the molecules of interest in vacuum and acetonitrile. The DFT-based optimized geometry of $[Ru(bpy)_3]^{2+}$ and its heterogenized analogue as linked with graphene through pyrazine linker ($[Ru(bpy)_3]^{2+}$–G_r) are displayed in Fig. 2. Table 1 comprises all the structural properties of the studied compounds of ruthenium and iron. Significantly, as mentioned in the methodology, carrying out the calculations in various solvents is necessary to determine the ΔG^o of solvation required for redox potential calculation in acetonitrile as a solvent. It is worth noting the results in Table 1 demonstrate that the impact of solvation on the structural properties of the studied system is insignificant; this comprises major bond length and angles of atoms. Interestingly, these DFT results demonstrate that heterogenization has a negligible impact on the key structural properties of the molecular complexes. The coordinates of all optimized geometries are provided in the supplementary information.

Furthermore, one may anticipate that such conjugated linkage between these $[Ru(bpy)_3]^{2+}$ complexes and graphene has an insignificant impact on molecular properties associated with the geometry of these complexes, such as electrochemical catalytic behavior and electroluminescence applications. For example, the DFT calculation revealed bond lengths for M–N bond of an average of 2.118, 2.112, and 2.024, 2.017 Å for Ru and Fe, respectively, in vacuum and acetonitrile, respectively. Importantly, comparing the effect of heterogenization on structural properties of examined molecules, i.e. $[M(bpy)_3]^{2+}$–G_r, M = Fe, Ru, one can notice a negligible effect on the main molecular properties. For example, an average bond length of 2.112 and 2.114 Å for Ru-N were calculated for the homogeneous and heterogeneous complexes, respectively.

Reduction potentials. The bpy-based Ru complexes can exhibit a variety of molecular properties that have recently attracted growing interests. A key feature of these Ruthenium complex is related to its redox properties that have been applied in a wide spectrum of applications, such as redox mediator–water oxidation catalyst and photoredox catalysis [71,72]. Hence, examining the effect of heterogenization on the reduction potential of $[M(bpy)_3]^{2+}$ is essential toward screening for more efficient heterogeneous molecular catalysts. Thus, as presented in the methodology, the redox potentials of the complexes considered in this study were calculated employing the Born-Haber cycle using the optimized geometries of all molecules simulated at the same level of the theory. Additionally, the determination of reduction potentials (vs. standard calomel electrode, SCE) was calculated for the molecular model $[M(bpy)_3]^{+2/1}$ and $[M(bpy)_3]^{+1/0}$ [M: Fe, Ru] before and after heterogenization. Table 2 summarizes the calculated standard one-electron reduction potential, E°_{red} in V for all species. Importantly, the calculated E^o_{red} was determined in acetonitrile implementing IEFPCM implicit solvation approach [67]. It is noteworthy mentioning that the DFT results concerning the reduction potential were validated via benchmarking with the experimental values wherever applicable as reported in the literature. Concerning the appropriateness of the DFT/B3LYP/IEFPCM method, various research groups reported different mean deviations for the calculated E^o_{red} of various series of metal complexes. For example, Roy et al. and Liang et al. reported mean deviations of ~ 0.16 and 0.23 V for selected metal complexes. To this end, as can be noted in Table 2, the DFT calculation revealed E^o_{red} of -1.21 and -1.85 V for the homogeneous molecular catalysts of $[Ru(bpy)_3]^{2+/1+}$ and $[Ru(bpy)_3]^{1+/0}$, respectively, which are in good agreement with the experimental value of -1.30 and -1.49 V of $[Ru(bpy)_3]^{2+/1+}$ and $[Ru(bpy)_3]^{1+/0}$, respectively, reported in the literature [67]. Henceforth, the same method of calculations at the same level of DFT theory was performed for the heterogenized molecular catalysts of Fe and Ru. In contrast to $[Ru(bpy)_3]^{2+/1+}$-G_r, $[Ru(bpy)_3]^{2+}$potential was -1.21 V compared to -1.03 V in heterogeneous indicative of insignificant change. Also, the potentials of the same complexes form one to zero charged was -1.85 V for $[Ru(bpy)_3]^{2+}$ compared to -1.76 V in $[Ru(bpy)_3]^{1+/0}$–G_r.

Table 2
Computed first and second reduction potentials (E°_{red} vs. SCE) of Ru and Fe complexes and their graphene-based heterogeneous analogues in Acetonitrile.

Ru		
	E°_{red} (2+/1+), V	E°_{red} (1+/0), V
$[Ru(bpy)_3]^{2+}$	−1.21	−1.85
$[Ru(bpy)_3]^{2+}$-G_r	−1.03	−1.76
Fe		
	2+/1+	1+/0
$[Fe(bpy)_3]^{2+}$	−1.28	−1.94
$[Fe(bpy)_3]^{2+}$-G_r	−1.04	−1.78

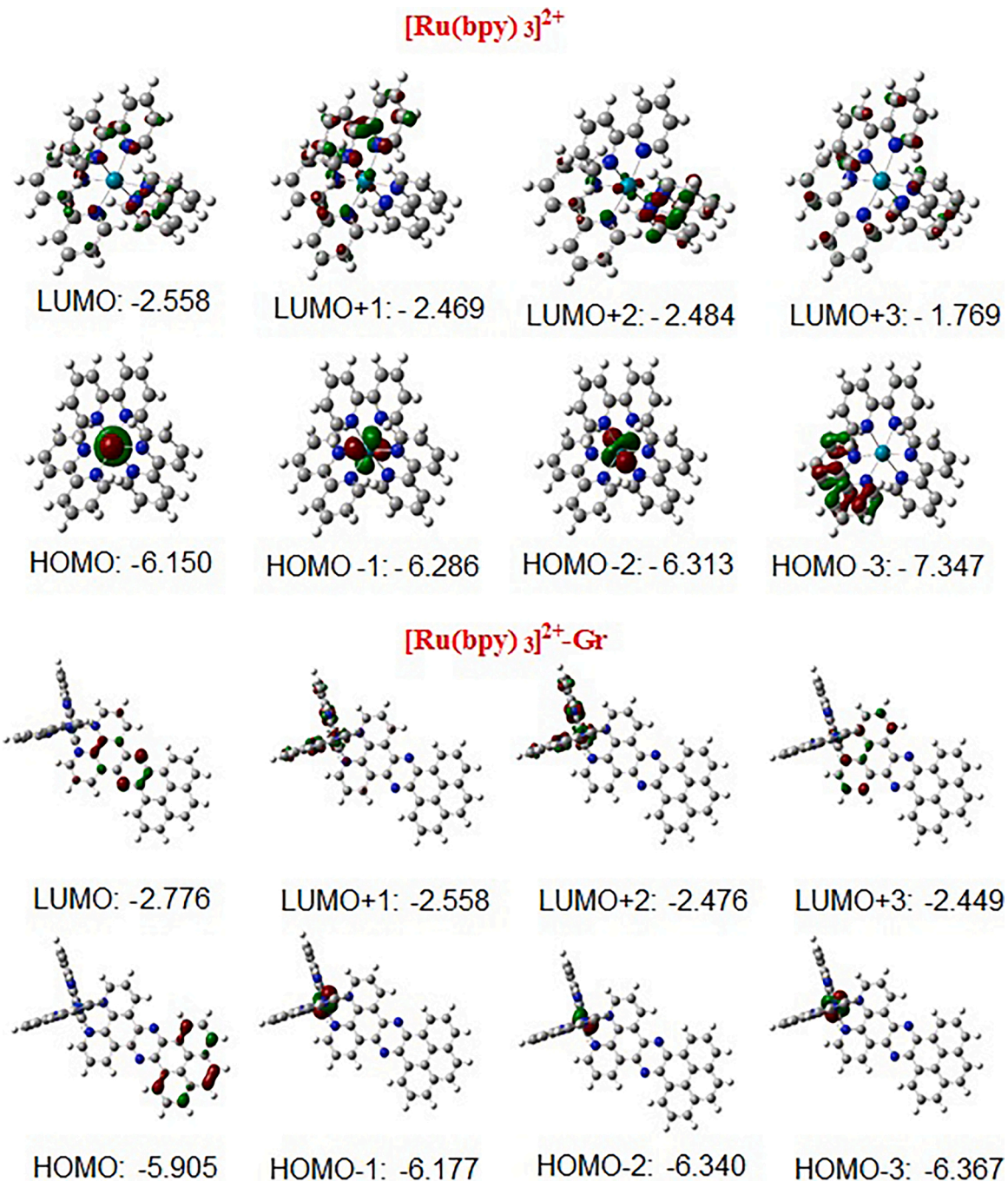

Fig. 3. Simulated selected MOs and the corresponding Energy (eV) of $[Ru(bpy)_3]^{2+}$ and $[Ru(bpy)_3]^{2+}$-G_r in acetonitrile.

Furthermore, the $[Ru(bpy)_3]^{2+/1+}$ and $[Fe(bpy)_3]^{2+/1+}$ calculated potentials were -1.21 and -1.28 V respectively. For $[Ru(bpy)_3]^{1+/0}$–G_r with $[Fe(bpy)_3]^{1+/0}$–G_r the potentials were -1.76, -1.78 V, which indicates that the change of the metal did not affect the reduction potentials of the catalyst. Furthermore, it is worth noting that the DFT calculations revealed that the graphene-based heterogenization of $[Ru(bpy)_3]^{2+}$ afforded a ΔE°_{red} of +0.18 V indicative of a temperate increasing oxidization strength that can be potentially important in photoredox catalysis and other applications.

Molecular orbitals. It is noteworthy mentioning that providing insights concerning the molecular orbitals (MOs) can be helpful toward understanding the characteristics of an electrocatalyst in terms of reactivity and efficiency. As a general principle, the frontier MOs, namely HOMO and LUMO, are involved in such an electrocatalytic process where a reduced value for the electrocatalyst's overpotential is desired. This can be generally assessed via investigating the effect of heterogenization on such MOs. To this end, DFT simulation of MOs of all complexes was conducted including HOMO-3: LUMO + 3. Hence, The MOs of the homogenous and heterogeneous complexes, $[Ru(bpy)_3]^{2+}$ and $[Ru(bpy)_3]^{2+}$-G_r, are examined in order to analyze the corresponding catalytic properties and the effect of the heterogenization on the catalyst. Selected MOs of Ru complexes before and after immobilization on graphene are illustrated in Fig. 3.

The general observation is that the MOs are stabilized upon heterogenization, which provides the opportunity to reduce the overpotential for the electrocatalysis process [73]. Examining Fig. 3 one can notice that the LUMO of $[Ru(bpy)_3]^{2+}$ is delocalized mainly over the bpy ligand with calculated energy of -2.558 eV. Upon heterogenization, the LUMO

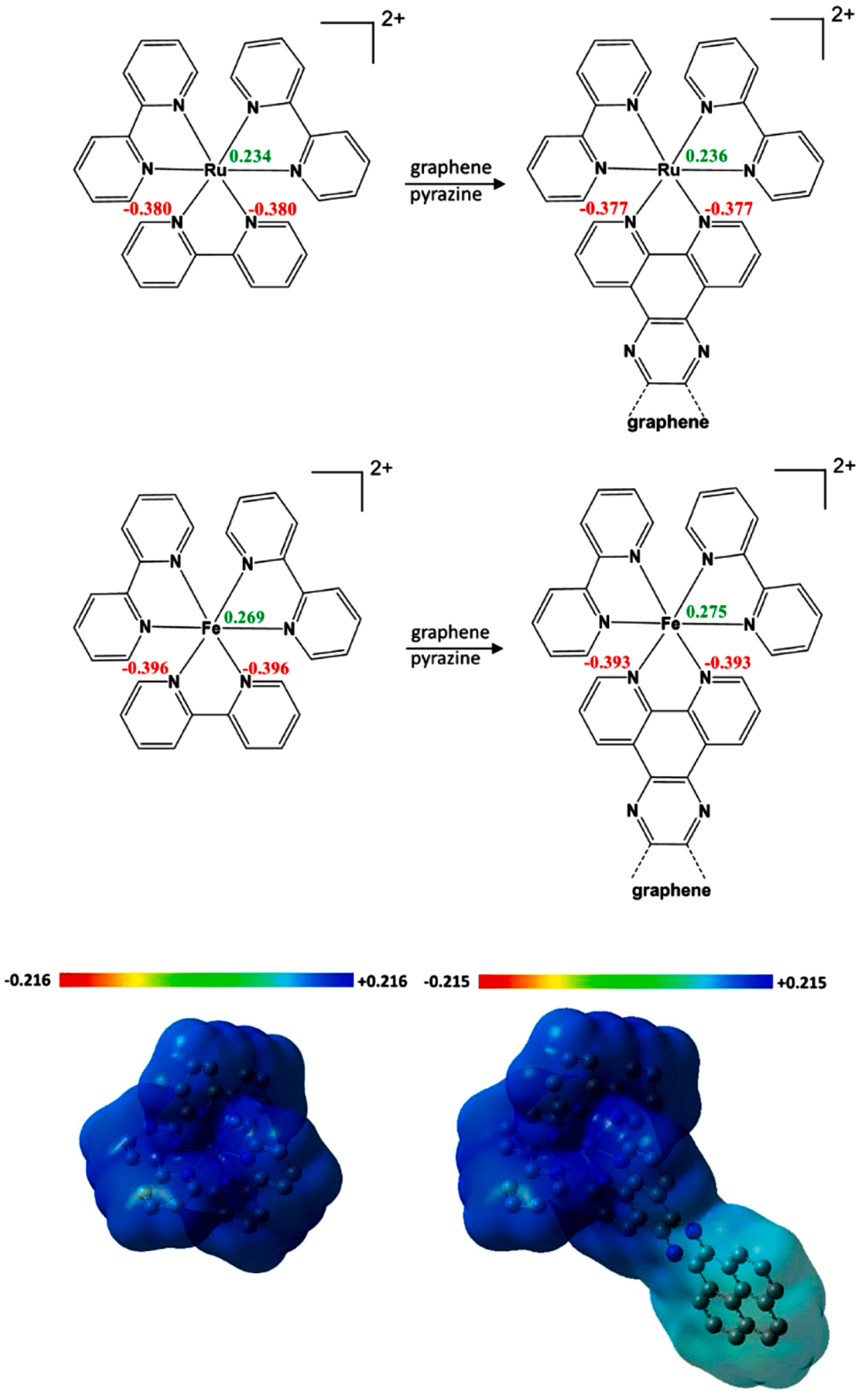

Fig. 4. Top: the NBO charges of the $[M(bpy)_3]^{2+}$ (M = Fe, Ru) complexes before and after heterogenization with graphene with pyrazine as a linker; bottom: the EPS maps of $[Ru(bpy)_3]^{2+}$ and $[Ru(bpy)_3]^{2+}$-Gr.

of $[Ru(bpy)_3]^{2+}$-G_r exhibited alike ligand-centered delocalization that comprises the pyrazine moiety with calculated energy of -2.776 eV indicative of stabilization by 0.218 eV. However, it is worth noting that although the LUMO of both species exhibits a ligand-centered delocalization, they are relatively different. The LUMO of $[Ru(bpy)_3]^{2+}$ has become LUMO-1 after heterogenization with the same energy of -2.558 eV, whereas the insertion of pyrazine after heterogenization afforded a new LUMO. In principle, as the 2+/1+ reduction of $[Ru(bpy)_3]^{2+}$, as an emerging consensus, is a ligand-centered process, these results suggest that both species can undergo a reduction process through a LUMO that exhibit a ligand-centered delocalization suggesting that the $[Ru(bpy)_3]^{2+}$ complex and the heterogenized counterpart

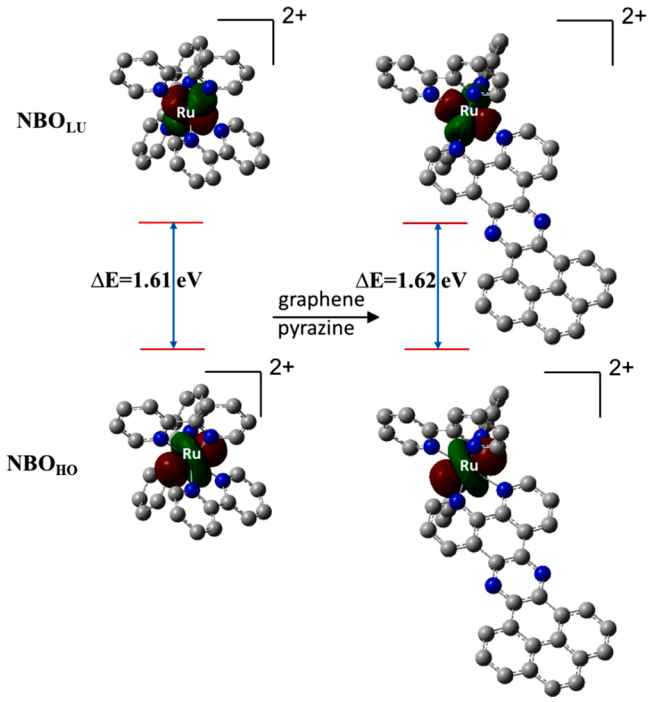

Fig. 5. The NBO_{HO} and NBO_{LU} of $[Ru(bpy)_3]^{2+}$ and $[Ru(bpy)_3]^{2+}$-Gr and the corresponding energy gap; $\Delta E(eV) = E(NBO_{LU} - NBO_{HO})$; hydrogen atoms are omitted for clarity.

may proceed through alike reductive catalytic pathways. On the other hand, one can notice that the MOs of $[Ru(bpy)_3]^{2+}$ undergo notable change upon heterogenization. HOMO, HOMO-1, and HOMO-2 are all metal-localized orbitals with calculated energy of -6.150, 6.286, and 6.313 eV, respectively. Upon heterogenization, a new HOMO is allocated that is ascribed as graphene-delocalized orbital with calculated energy of -5.595 eV, whereas an insignificant effect is noted for the other MOs. Thus, these results suggest that an oxidative catalytic process involving $[Ru(bpy)_3]^{2+}$ can be affected by the graphene-based heterogenization. Hence, generally speaking, these DFT-based calculations of the MOs suggest that $[Ru(bpy)_3]^{2+}$ and its graphene-based counterpart may exhibit comparative catalytic behavior upon being utilized as molecular catalysts for a wide range of chemical reactions of interest.

Natural Bond Orbital (NBO) Analysis. In principle, as stated earlier, the geometry optimization process is a necessary step toward further analysis where more information concerning the intramolecular bondings as well as intermolecular interaction is needed. In particular, the NBO analysis was performed herein to investigate the nature of the charge density associated with the graphene-based heterogenization of $[Ru(bpy)_3]^{2+}$. Fig. 4-top depicts the NBO charges for both complexes of Ru and Fe before and after graphene-based heterogenization.

The NBO analyses revealed a negligible change in the charge density (Δq) of 0.002 and 0.006 for the Ru and Fe centers as a result of graphene-based heterogenization, respectively. One can notice also that a Δq of only 0.003 was calculated for the nitrogen atoms in both complexes upon heterogenization with graphene indicative of insignificant change. On the other hand, it is noteworthy to mention that such a minor decrease in the NBO charge density can be attributed to the pyrazine linker, where an NBO charge of -0.427 is calculated for the nitrogen atoms for the Ru complexes. This variation in NBO charge density of the nitrogen atoms within the molecule $[Ru(bpy)_3]^{2+}$-Gr is illustrated in Fig. 4-bottom. It can be noted with the respect to the color codes that the pyrazine moiety can slightly alter the polarity of the whole molecule that can induce small change in the charge density within the metal and nitrogen centers of the metal complexes.

Furthermore, it is necessary not only to examine the NBO charges of a molecule of interest but also it is essential to investigate the nature and types of such NBOs. Fig. 5 displays the major NBOs of $[Ru(bpy)_3]^{2+}$ and $[Ru(bpy)_3]^{2+}$-Gr and the corresponding energy gap. Examining Fig. 5, one can notice that the highest occupied NBO (NBO_{HO}) is ascribed to the d_z2 orbital of the metal center, whereas the lowest unoccupied NBO (NBO_{LU}) is ascribed to the unoccupied d_{xz} orbital of the same metal center. It is worth noting that these ascriptions of NBO_{HO} and NBO_{LU} are analogous to the HOMO and LUMO of the molecule, respectively. The DFT calculations revealed an energy gap ($\Delta E(eV) = E(NBO_{LU} - NBO_{HO})$) of 1.61 and 3.26 eV for $[Ru(bpy)_3]^{2+}$ and $[Fe(bpy)_3]^{2+}$, respectively. With the lower value of ΔE obtained for $[Ru(bpy)_3]^{2+}$, these DFT calculations suggest that $[Ru(bpy)_3]^{2+}$ can exhibit relatively enhanced catalytic performance compared to the Fe counterpart. Interestingly, as one can notice from Fig. 5, the ΔE is not affected for both complexes

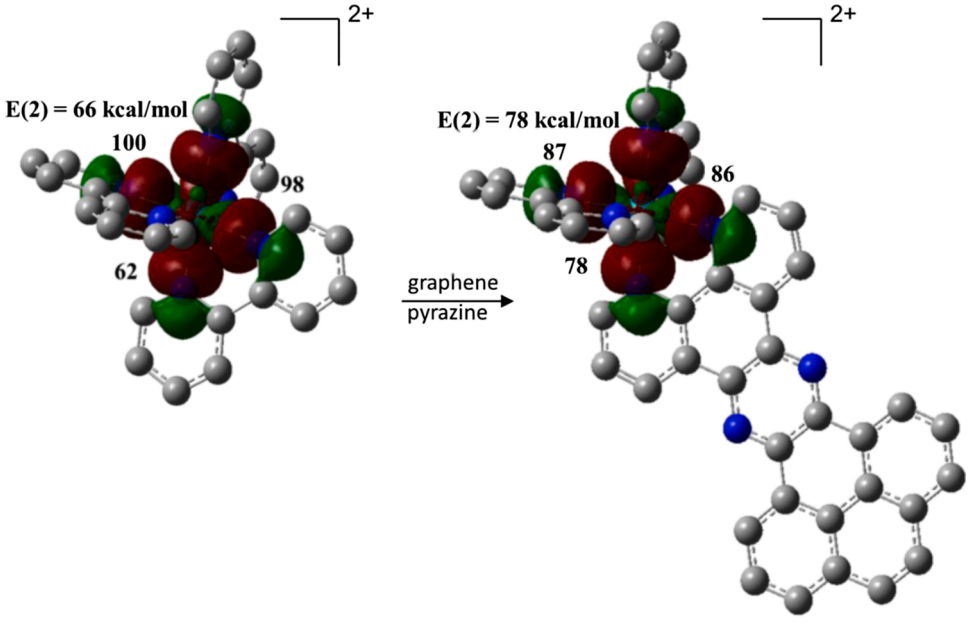

Fig. 6. The superposition of the NBOs of the major contributor of the lp(N)→ d_{xz}-LAO(Ru) transitions and the corresponding energy of interaction (E(2)) for $[Ru(bpy)_3]^{2+}$ and $[Ru(bpy)_3]^{2+}$-Gr. Hydrogen atoms were omitted for clarity.

concerning the effect the graphene-based heterogenization. As such, it is expected based on the obtained DFT results that the graphene-heterogenized counterpart of $[Ru(bpy)_3]^{2+}$ can exhibit comparable catalytic behavior compared to the homogeneous analogue. We further utilized the DFT results of the NBO analysis to examine any potential charge transfer between any given pair of orbitals amongst the NBOs of the examined molecules. Such a kind of potential charge transfer was evaluated employing the second perturbation energy of interaction (E (2)). Fig. 6 depicts the superposition of the NBOs accounted for the four charge transfers obtained from the NBO analyses. These four transitions were selected per a threshold of $E(2) \geq 20$ kcal/mol. It is worth noting that these superpositions of the NBOs accounted for the four charge transfers obtained from the NBO analyses. These four transitions were selected per a threshold of $E(2) \geq 20$ kcal/mol.

It is worth noting that these four transitions are attributed to the same type of transition namely the lone-pair of the N atoms of the bpy ligand to the unoccupied d_{xz} orbital of the metal atom, which is ascribed as lp(N)→ d_{xz}-LAO(M). As illustrated in Fig. 6, the DFT results revealed that both $[Ru(bpy)_3]^{2+}$ and $[Ru(bpy)_3]^{2+}$-Gr exhibit alike behavior concerning the types of the intramolecular NBO charge transfer with substantial averaged stabilizing energy E(2) of 81.5 and 82.3 kcal/mol, respectively. Furthermore, it is noteworthy to mention that we observed no difference between Ru and Fe concerning their NBO analyses. These DFT results suggest that there is no effect for the graphene-based heterogenization of the examined molecules. As such, it is expected that both forms of the molecules may exhibit alike catalytic performance.

4. Conclusions

Using DFT-based calculations in an implicit solvation model of acetonitrile, we have systematically investigated the redox and molecular properties of graphene-based covalently heterogenized molecular catalysts of $[M(bpy)_3]^{2+}$-G_r (M = Ru, Fe). The DFT results suggest that the heterogenized counterpart can exhibit redox and molecular properties that are well in line with the homogeneous analogues. As revealed by the DFT-optimized geometries of the examined species, the key structural properties of the complexes are not disturbed by heterogenization. On the other hand, for $[Ru(bpy)_3]^{2+}$, the DFT-based calculation revealed a ΔE°_{red} of 0.18 V upon heterogenization. As such, it can be suggested that both species, namely the homogeneous and the heterogenized counterpart of $[Ru(bpy)_3]^{2+}$, may undergo a similar reductive manner. Importantly, the results obtained by the MO and NBO analyses are well in line with the redox behaviors of both species. In particular, obtained results revealed that the LUMO of both analogues exhibits a ligand-centered delocalization suggestive of similar reductive-based catalytic pathways upon being utilized as molecular catalysts. Interestingly, the results reported herein be potentially utilized in future efforts toward designing novel and more efficient heterogeneous molecular catalysts.

Declaration of Competing Interest

The authors declare no competing interests

Acknowledgments

The support received from Qatar University is thankfully acknowledged. The calculations were performed using the supercomputing facility at the Texas A&M University at Qatar. Open Access funding provided by the Qatar National Library

Appendix A. Supplementary data

Supplementary material related to this article can be found, in the online version, at doi:https://doi.org/10.1016/j.mtcomm.2020.101694.

References

[1] K.J. Lee, N. Elgrishi, B. Kandemir, J.L. Dempsey, Electrochemical and spectroscopic methods for evaluating molecular electrocatalysts, Int. Rev. Chem. Eng. 1 (2017), https://doi.org/10.1038/s41570-017-0039, 0039.
[2] S. Ren, D. Joulié, D. Salvatore, K. Torbensen, M. Wang, M. Robert, C. P. Berlinguette, Molecular electrocatalysts can mediate fast, selective CO 2 reduction in a flow cell, Science 365 (80) (2019) 367–369, https://doi.org/10.1126/science.aax4608.
[3] C. Costentin, J.-M. Savéant, Towards an intelligent design of molecular electrocatalysts, Int. Rev. Chem. Eng. 1 (2017), https://doi.org/10.1038/s41570-017-0087, 0087.
[4] S. Hammes-Schiffer, Controlling electrons and protons through theory: molecular electrocatalysts to nanoparticles, Acc. Chem. Res. 51 (2018) 1975–1983, https://doi.org/10.1021/acs.accounts.8b00240.
[5] R. Francke, B. Schille, M. Roemelt, Homogeneously catalyzed electroreduction of carbon dioxide - methods, mechanisms, and catalysts, Chem. Rev. 118 (2018) 4631–4701, https://doi.org/10.1021/acs.chemrev.7b00459.
[6] R.M. Bullock, M.L. Helm, Molecular electrocatalysts for oxidation of hydrogen using earth-abundant metals: shoving protons around with proton relays, Acc. Chem. Res. 48 (2015) 2017–2026, https://doi.org/10.1021/acs.accounts.5b00069.
[7] A.W. Cook, K.M. Waldie, Molecular electrocatalysts for alcohol oxidation: insights and challenges for catalyst design, ACS Appl. Energy Mater. 3 (2020) 38–46, https://doi.org/10.1021/acsaem.9b01820.
[8] N.X. Gu, P.H. Oyala, J.C. Peters, H 2 evolution from a thiolate-bound Ni(III) hydride, J. Am. Chem. Soc. 142 (2020) 7827–7835, https://doi.org/10.1021/jacs.0c00712.
[9] F. Li, A. Thevenon, A. Rosas-Hernández, Z. Wang, Y. Li, C.M. Gabardo, A. Ozden, C. T. Dinh, J. Li, Y. Wang, J.P. Edwards, Y. Xu, C. McCallum, L. Tao, Z.-Q. Liang, M. Luo, X. Wang, H. Li, C.P. O'Brien, C.-S. Tan, D.-H. Nam, R. Quintero-Bermudez, T.-T. Zhuang, Y.C. Li, Z. Han, R.D. Britt, D. Sinton, T. Agapie, J.C. Peters, E. H. Sargent, Molecular tuning of CO2-to-ethylene conversion, Nature 577 (2020) 509–513, https://doi.org/10.1038/s41586-019-1782-2.
[10] H.-F. Wang, L. Chen, H. Pang, S. Kaskel, Q. Xu, MOF-derived electrocatalysts for oxygen reduction, oxygen evolution and hydrogen evolution reactions, Chem. Soc. Rev. 49 (2020) 1414–1448, https://doi.org/10.1039/C9CS00906J.
[11] P. Trogadas, M.-O. Coppens, Nature-inspired electrocatalysts and devices for energy conversion, Chem. Soc. Rev. 49 (2020) 3107–3141, https://doi.org/10.1039/C8CS00797G.
[12] J. Zhu, A. Abdelkader, D. Demko, L. Deng, P. Zhang, T. He, Y. Wang, L. Huang, Electrocatalytic assisted performance enhancement for the Na-S battery in Nitrogen-Doped Carbon Nanospheres Loaded with Fe, Molecules 25 (2020) 1585, https://doi.org/10.3390/molecules25071585.
[13] X.F. Lu, B.Y. Xia, S. Zang, X.W. (David) Lou, Metal–Organic frameworks based electrocatalysts for the oxygen reduction reaction, Angew. Chemie Int. Ed. 59 (2020) 4634–4650, https://doi.org/10.1002/anie.201910309.
[14] H. Sun, Z. Yan, F. Liu, W. Xu, F. Cheng, J. Chen, Self-supported transition-metal-Based electrocatalysts for hydrogen and oxygen evolution, Adv. Mater. 32 (2020) 1806326, https://doi.org/10.1002/adma.201806326.
[15] J.A. Trindell, Z. Duan, G. Henkelman, R.M. Crooks, Well-defined nanoparticle electrocatalysts for the refinement of theory, Chem. Rev. 120 (2020) 814–850, https://doi.org/10.1021/acs.chemrev.9b00246.
[16] D. Gao, I. Trentin, L. Schwiedrzik, L. González, C. Streb, The reactivity and stability of polyoxometalate water oxidation electrocatalysts, Molecules 25 (2019) 157, https://doi.org/10.3390/molecules25010157.
[17] J. Song, C. Wei, Z.-F. Huang, C. Liu, L. Zeng, X. Wang, Z.J. Xu, A review on fundamentals for designing oxygen evolution electrocatalysts, Chem. Soc. Rev. 49 (2020) 2196–2214, https://doi.org/10.1039/C9CS00607A.
[18] J. Zhu, L. Hu, P. Zhao, L.Y.S. Lee, K.-Y. Wong, Recent Advances in Electrocatalytic Hydrogen Evolution Using Nanoparticles, Chem. Rev. 120 (2020) 851–918, https://doi.org/10.1021/acs.chemrev.9b00248.
[19] H. Zhong, M. Ghorbani-Asl, K.H. Ly, J. Zhang, J. Ge, M. Wang, Z. Liao, D. Makarov, E. Zschech, E. Brunner, I.M. Weidinger, J. Zhang, A.V. Krasheninnikov, S. Kaskel, R. Dong, X. Feng, Synergistic electroreduction of carbon dioxide to carbon monoxide on bimetallic layered conjugated metal-organic frameworks, Nat. Commun. 11 (2020) 1409, https://doi.org/10.1038/s41467-020-15141-y.
[20] F. Podjaski, D. Weber, S. Zhang, L. Diehl, R. Eger, V. Duppel, E. Alarcón-Lladó, G. Richter, F. Haase, A. Fontcuberta i Morral, C. Scheu, B.V. Lotsch, Rational strain engineering in delafossite oxides for highly efficient hydrogen evolution catalysis in acidic media, Nat. Catal. 3 (2020) 55–63, https://doi.org/10.1038/s41929-019-0400-x.
[21] A.K. Geim, K.S. Novoselov, The rise of graphene, Nat. Mater. 6 (2007) 183–191, https://doi.org/10.1038/nmat1849.
[22] K.S. Kim, Y. Zhao, H. Jang, S.Y. Lee, J.M. Kim, K.S. Kim, J.-H. Ahn, P. Kim, J.-Y. Choi, B.H. Hong, Large-scale pattern growth of graphene films for stretchable transparent electrodes, Nature 457 (2009) 706–710, https://doi.org/10.1038/nature07719.
[23] Y. Zhu, S. Murali, W. Cai, X. Li, J.W. Suk, J.R. Potts, R.S. Ruoff, Graphene and Graphene Oxide: Synthesis, Properties, and Applications, Adv. Mater. 22 (2010) 3906–3924, https://doi.org/10.1002/adma.201001068.
[24] C. Backes, A.M. Abdelkader, C. Alonso, A. Andrieux-Ledier, R. Arenal, J. Azpeitia, N. Balakrishnan, L. Banszerus, J. Barjon, R. Bartali, S. Bellani, C. Berger, R. Berger, M.M.B. Ortega, C. Bernard, P.H. Beton, A. Beyer, A. Bianco, P. Bøggild, F. Bonaccorso, G.B. Barin, C. Botas, R.A. Bueno, D. Carriazo, A. Castellanos-Gomez, M. Christian, A. Ciesielski, T. Ciuk, M.T. Cole, J. Coleman, C. Coletti, L. Crema, H. Cun, D. Dasler, D. De Fazio, N. Díez, S. Drieschner, G.S. Duesberg, R. Fasel,

X. Feng, A. Fina, S. Forti, C. Galiotis, G. Garberoglio, J.M. García, J.A. Garrido, M. Gibertini, A. Gölzhäuser, J. Gómez, T. Greber, F. Hauke, A. Hemmi, I. Hernandez-Rodriguez, A. Hirsch, S.A. Hodge, Y. Huttel, P.U. Jepsen, I. Jimenez, U. Kaiser, T. Kaplas, H. Kim, A. Kis, K. Papagelis, K. Kostarelos, A. Krajewska, K. Lee, C. Li, H. Lipsanen, A. Liscio, M.R. Lohe, A. Loiseau, L. Lombardi, M. Francisca López, O. Martin, C. Martín, L. Martínez, J.A. Martin-Gago, J. Ignacio Martínez, N. Marzari, Á. Mayoral, J. McManus, M. Melucci, J. Méndez, C. Merino, P. Merino, A.P. Meyer, E. Miniussi, V. Miseikis, N. Mishra, V. Morandi, C. Munuera, R. Muñoz, H. Nolan, L. Ortolani, A.K. Ott, I. Palacio, V. Palermo, J. Parthenios, I. Pasternak, A. Patane, M. Prato, H. Prevost, V. Prudkovskiy, N. Pugno, T. Rojo, A. Rossi, P. Ruffieux, P. Samorì, L. Schué, E. Setijadi, T. Seyller, G. Speranza, C. Stampfer, I. Stenger, W. Strupinski, Y. Svirko, S. Taioli, K.B.K. Teo, M. Testi, F. Tomarchio, M. Tortello, E. Treossi, A. Turchanin, E. Vazquez, E. Villaro, P. R. Whelan, Z. Xia, R. Yakimova, S. Yang, G.R. Yazdi, C. Yim, D. Yoon, X. Zhang, X. Zhuang, L. Colombo, A.C. Ferrari, M. Garcia-Hernandez, Production and processing of graphene and related materials, 2d Mater. 7 (2020) 022001, https://doi.org/10.1088/2053-1583/ab1e0a.

[25] S. Stankovich, D.A. Dikin, G.H.B. Dommett, K.M. Kohlhaas, E.J. Zimney, E. A. Stach, R.D. Piner, S.T. Nguyen, R.S. Ruoff, Graphene-based composite materials, Nature 442 (2006) 282–286, https://doi.org/10.1038/nature04969.

[26] A.K. Geim, Graphene: status and prospects, Science 324 (80) (2009) 1530–1534, https://doi.org/10.1126/science.1158877.

[27] K.S. Novoselov, V.I. Fal′ko, L. Colombo, P.R. Gellert, M.G. Schwab, K. Kim, A roadmap for graphene, Nature. 490 (2012) 192–200, https://doi.org/10.1038/nature11458.

[28] X. Li, W. Cai, J. An, S. Kim, J. Nah, D. Yang, R. Piner, A. Velamakanni, I. Jung, E. Tutuc, S.K. Banerjee, L. Colombo, R.S. Ruoff, Large-area synthesis of high-quality and uniform graphene films on copper foils, Science 324 (80) (2009) 1312–1314, https://doi.org/10.1126/science.1171245.

[29] C. Su, M. Acik, K. Takai, J. Lu, S. Hao, Y. Zheng, P. Wu, Q. Bao, T. Enoki, Y. J. Chabal, K. Ping Loh, Probing the catalytic activity of porous graphene oxide and the origin of this behaviour, Nat. Commun. 3 (2012) 1298, https://doi.org/10.1038/ncomms2315.

[30] B.F. Machado, P. Serp, Graphene-based materials for catalysis, Catal. Sci. Technol. 2 (2012) 54–75, https://doi.org/10.1039/C1CY00361E.

[31] M. Hu, Z. Yao, X. Wang, Graphene-based nanomaterials for catalysis, Ind. Eng. Chem. Res. 56 (2017) 3477–3502, https://doi.org/10.1021/acs.iecr.6b05048.

[32] J. Duan, S. Chen, M. Jaroniec, S.Z. Qiao, Heteroatom-doped graphene-based materials for energy-relevant electrocatalytic processes, ACS Catal. 5 (2015) 5207–5234, https://doi.org/10.1021/acscatal.5b00991.

[33] H. He, Z. Li, K. Li, G. Lei, X. Guan, G. Zhang, F. Zhang, X. Fan, W. Peng, Y. Li, Bifunctional graphene-based metal-free catalysts for oxidative coupling of amines, ACS Appl. Mater. Interfaces 11 (2019) 31844–31850, https://doi.org/10.1021/acsami.9b08741.

[34] D. Deng, K.S. Novoselov, Q. Fu, N. Zheng, Z. Tian, X. Bao, Catalysis with two-dimensional materials and their heterostructures, Nat. Nanotechnol. 11 (2016) 218–230, https://doi.org/10.1038/nnano.2015.340.

[35] B. Qiu, M. Xing, J. Zhang, Recent advances in three-dimensional graphene based materials for catalysis applications, Chem. Soc. Rev. 47 (2018) 2165–2216, https://doi.org/10.1039/C7CS00904F.

[36] X.-K. Kong, C.-L. Chen, Q.-W. Chen, Doped graphene for metal-free catalysis, Chem. Soc. Rev. 43 (2014) 2841–2857, https://doi.org/10.1039/C3CS60401B.

[37] S. Zhu, J. Wang, W. Fan, Graphene-based catalysis for biomass conversion, Catal. Sci. Technol. 5 (2015) 3845–3858, https://doi.org/10.1039/C5CY00339C.

[38] P. Kuang, M. Sayed, J. Fan, B. Cheng, J. Yu, 3D graphene-based H 2 -production photocatalyst and electrocatalyst, Adv. Energy Mater. 10 (2020) 1903802, https://doi.org/10.1002/aenm.201903802.

[39] X. Peng, Y. Zen, Q. Liu, L. Liu, H. Wang, Graphene oxide as a green carbon material for cross-coupling of indoles with ethers: via oxidation and the Friedel-Crafts reaction, Org. Chem. Front. (2019), https://doi.org/10.1039/c9qo00926d.

[40] F.M. Koehler, W.J. Stark, Organic synthesis on graphene, Acc. Chem. Res. 46 (2013) 2297–2306, https://doi.org/10.1021/ar300125w.

[41] Y. Li, W. Zhou, H. Wang, L. Xie, Y. Liang, F. Wei, J.-C. Idrobo, S.J. Pennycook, H. Dai, An oxygen reduction electrocatalyst based on carbon nanotube–graphene complexes, Nat. Nanotechnol. 7 (2012) 394–400, https://doi.org/10.1038/nnano.2012.72.

[42] Y. Liang, Y. Li, H. Wang, J. Zhou, J. Wang, T. Regier, H. Dai, Co3O4 nanocrystals on graphene as a synergistic catalyst for oxygen reduction reaction, Nat. Mater. 10 (2011) 780–786, https://doi.org/10.1038/nmat3087.

[43] L. Qu, Y. Liu, J.-B. Baek, L. Dai, Nitrogen-Doped Graphene as Efficient Metal-Free Electrocatalyst for Oxygen Reduction in Fuel Cells, ACS Nano 4 (2010) 1321–1326, https://doi.org/10.1021/nn901850u.

[44] Y. Zheng, Y. Jiao, Y. Zhu, L.H. Li, Y. Han, Y. Chen, A. Du, M. Jaroniec, S.Z. Qiao, Hydrogen evolution by a metal-free electrocatalyst, Nat. Commun. 5 (2014) 3783, https://doi.org/10.1038/ncomms4783.

[45] J.-S. Li, Y. Wang, C.-H. Liu, S.-L. Li, Y.-G. Wang, L.-Z. Dong, Z.-H. Dai, Y.-F. Li, Y.-Q. Lan, Coupled molybdenum carbide and reduced graphene oxide electrocatalysts for efficient hydrogen evolution, Nat. Commun. 7 (2016) 11204, https://doi.org/10.1038/ncomms11204.

[46] A. Xie, N. Xuan, K. Ba, Z. Sun, Pristine graphene electrode in hydrogen evolution reaction, ACS Appl. Mater. Interfaces 9 (2017) 4643–4648, https://doi.org/10.1021/acsami.6b14732.

[47] H.-C. Hsu, I. Shown, H.-Y. Wei, Y.-C. Chang, H.-Y. Du, Y.-G. Lin, C.-A. Tseng, C.-H. Wang, L.-C. Chen, Y.-C. Lin, K.-H. Chen, Graphene oxide as a promising photocatalyst for CO 2 to methanol conversion, Nanoscale. 5 (2013) 262–268, https://doi.org/10.1039/C2NR31718D.

[48] C. Zhang, S. Yang, J. Wu, M. Liu, S. Yazdi, M. Ren, J. Sha, J. Zhong, K. Nie, A. S. Jalilov, Z. Li, H. Li, B.I. Yakobson, Q. Wu, E. Ringe, H. Xu, P.M. Ajayan, J. M. Tour, Electrochemical CO 2 reduction with atomic iron-dispersed on nitrogen-doped graphene, Adv. Energy Mater. 8 (2018) 1703487, https://doi.org/10.1002/aenm.201703487.

[49] J.D. Blakemore, A. Gupta, J.J. Warren, B.S. Brunschwig, H.B. Gray, Noncovalent immobilization of electrocatalysts on carbon electrodes for fuel production, J. Am. Chem. Soc. 135 (2013) 18288–18291, https://doi.org/10.1021/ja4099609.

[50] R.M. Bullock, A.K. Das, A.M. Appel, Surface immobilization of molecular electrocatalysts for energy conversion, Chem. - A Eur. J. 23 (2017) 7626–7641, https://doi.org/10.1002/chem.201605066.

[51] A. Das, S.S. Stahl, Noncovalent immobilization of molecular electrocatalysts for chemical synthesis: efficient electrochemical alcohol oxidation with a Pyrene-TEMPO conjugate, Angew. Chemie Int. Ed. 56 (2017) 8892–8897, https://doi.org/10.1002/anie.201704921.

[52] M.F. Kuehnel, K.L. Orchard, K.E. Dalle, E. Reisner, Selective photocatalytic CO 2 reduction in water through anchoring of a molecular Ni catalyst on CdS nanocrystals, J. Am. Chem. Soc. 139 (2017) 7217–7223, https://doi.org/10.1021/jacs.7b00369.

[53] S. Oh, J.R. Gallagher, J.T. Miller, Y. Surendranath, Graphite-conjugated rhenium catalysts for carbon dioxide reduction, J. Am. Chem. Soc. 138 (2016) 1820–1823, https://doi.org/10.1021/jacs.5b13080.

[54] Y. Zhao, G. Yu, F. Wang, P. Wei, J. Liu, Bioinspired transition-metal complexes as electrocatalysts for the oxygen reduction reaction, Chem. – A Eur. J. 25 (2019) 3726–3739, https://doi.org/10.1002/chem.201803764.

[55] M.N. Jackson, S. Oh, C.J. Kaminsky, S.B. Chu, G. Zhang, J.T. Miller, Y. Surendranath, Strong electronic coupling of molecular sites to graphitic electrodes via pyrazine conjugation, J. Am. Chem. Soc. 140 (2018) 1004–1010, https://doi.org/10.1021/jacs.7b10723.

[56] A.T. Lawal, Progress in utilisation of graphene for electrochemical biosensors, Biosens. Bioelectron. 106 (2018) 149–178, https://doi.org/10.1016/j.bios.2018.01.030.

[57] S. Oh, J.R. Gallagher, J.T. Miller, Y. Surendranath, Graphite-conjugated rhenium catalysts for carbon dioxide reduction, J. Am. Chem. Soc. 138 (2016) 1820–1823, https://doi.org/10.1021/jacs.5b13080.

[58] A. Devadoss, C.E.D. Chidsey, Azide-modified graphitic surfaces for covalent attachment of alkyne-terminated molecules by “Click” chemistry, J. Am. Chem. Soc. 129 (2007) 5370–5371, https://doi.org/10.1021/ja071291f.

[59] S. Li, X. Zhong, H. Yang, Y. Hu, F. Zhang, Z. Niu, W. Hu, Z. Dong, J. Jin, R. Li, J. Ma, Noncovalent modified graphene sheets with ruthenium(II) complexes used as electrochemiluminescent materials and photosensors, Carbon 49 (2011) 4239–4245, https://doi.org/10.1016/j.carbon.2011.05.058.

[60] J. Malig, N. Jux, D.M. Guldi, Toward multifunctional wet chemically functionalized graphene—integration of oligomeric, molecular, and particulate building blocks that reveal photoactivity and redox activity, Acc. Chem. Res. 46 (2013) 53–64, https://doi.org/10.1021/ar300124z.

[61] G.E. Frisch, M. J. Trucks, G. W. Schlegel, H. B. Scuseria, V. M. Robb, M. A. Cheeseman, J. R.; Scalmani, G.; Barone, H. B.; Petersson, G. A.; Nakatsuji, H.; Caricato, M.; Li, X.; Hratchian, M.. P.; Izmaylov, A. F.; Bloino, J.; Zheng, G.; Sonnenberg, J. L.; Hada, M.. N. Ehara, M.; Toyota, K.; Fukuda, R.; Hasegawa, J.; Ishida, J.. T.; Honda, Y.; Kitao, O.; Nakai, H.; Vreven, T.; Montgomery, J. A., E.N.. Peralta, J. E.; Ogliaro, F.; Bearpark, M. J.; Heyd, J.; Brothers, J.. Kudin, K. N.; Staroverov, V. N.; Kobayashi, R.; Normand, S.S.. Raghavachari, K.; Rendell, A. P.; Burant, J. C.; Iyengar, J.E.. Tomasi, J.; Cossi, M.; Rega, N.; Millam, N. J.; Klene, M.; Knox, R.. Cross, J. B.; Bakken, V.; Adamo, C.; Jaramillo, J.; Gomperts, C.. Stratmann, R. E.; Yazyev, O.; Austin, A. J.; Cammi, R.; Pomelli, V.G.. Ochterski, J. W.; Martin, R. L.; Morokuma, K.; Zakrzewski, A. Voth, G. A.; Salvador, P.; Dannenberg, J. J.; Dapprich, S.; Daniels, D.J. D.; Farkas, O.; Foresman, J. B.; Ortiz, J. V.; Cioslowski, J.; Fox, Gaussian 09., Gaussian, Inc. Wallingford, CT,. (n.d.).

[62] J. Tomasi, B. Mennucci, E. Cancès, The IEF version of the PCM solvation method: an overview of a new method addressed to study molecular solutes at the QM ab initio level, J. Mol. Struct. THEOCHEM. 464 (1999) 211–226, https://doi.org/10.1016/S0166-1280(98)00553-3.

[63] S.E. Jerng, B. Chang, H. Shin, H. Kim, T. Lee, K. Char, J.W. Choi, Pyrazine-linked 2D covalent organic frameworks as coating material for high-nickel layered oxide cathodes in lithium-ion batteries, ACS Appl. Mater. Interfaces 12 (2020) 10597–10606, https://doi.org/10.1021/acsami.0c00643.

[64] N.D. Ricke, A.T. Murray, J.J. Shepherd, M.G. Welborn, T. Fukushima, T. Van Voorhis, Y. Surendranath, Molecular-level insights into oxygen reduction catalysis by graphite-conjugated active sites, ACS Catal. (2017), https://doi.org/10.1021/acscatal.7b03086.

[65] R. Sharma, J.H. Baik, C.J. Perera, M.S. Strano, Anomalously large reactivity of single graphene layers and edges toward Electron transfer chemistries, Nano Lett. 10 (2010) 398–405, https://doi.org/10.1021/nl902741x.

[66] R. Sharma, N. Nair, M.S. Strano, Structure−Reactivity relationships for graphene nanoribbons, J. Phys. Chem. C. 113 (2009) 14771–14777, https://doi.org/10.1021/jp904814h.

[67] G. Liang, N.J. DeYonker, X. Zhao, C.E. Webster, Prediction of the reduction potential in transition-metal containing complexes: how expensive? For what accuracy? J. Comput. Chem. 38 (2017) 2430–2438, https://doi.org/10.1002/jcc.24894.

[68] A.D. Bani-Yaseen, E. Elbashier, Computational insights on the electrocatalytic behavior of [Cp*Rh] molecular catalysts immobilized on graphene for heterogeneous hydrogen evolution reaction, Sci. Rep. 10 (2020) 1–10, https://doi.org/10.1038/s41598-020-62758-6.

[69] M. Namazian, C.Y. Lin, M.L. Coote, Benchmark calculations of absolute reduction potential of Ferricinium/Ferrocene couple in nonaqueous solutions, J. Chem. Theory Comput. 6 (2010) 2721–2725, https://doi.org/10.1021/ct1003252.
[70] T. Fukushima, W. Drisdell, J. Yano, Y. Surendranath, Graphite-conjugated Pyrazines as molecularly tunable heterogeneous electrocatalysts, J. Am. Chem. Soc. 137 (2015) 10926–10929, https://doi.org/10.1021/jacs.5b06737.
[71] J.J. Concepcion, J.W. Jurss, P.G. Hoertz, T.J. Meyer, Catalytic and surface-electrocatalytic water oxidation by redox mediator-catalyst assemblies, Angew. Chemie Int. Ed. 48 (2009) 9473–9476, https://doi.org/10.1002/anie.200901279.
[72] J.W. Tucker, C.R.J. Stephenson, Shining light on photoredox catalysis: theory and synthetic applications, J. Org. Chem. 77 (2012) 1617–1622, https://doi.org/10.1021/jo202538x.
[73] S. Sato, K. Saita, K. Sekizawa, S. Maeda, T. Morikawa, Low-energy electrocatalytic CO2Reduction in water over Mn-Complex catalyst electrode aided by a nanocarbon support and K+Cations, ACS Catal. 8 (2018) 4452–4458, https://doi.org/10.1021/acscatal.8b01068.